Structural reorganization of non-cellulosic polymers observed in-situ during dilute acid pretreatment by small-angle neutron scattering

Zhi Yang[1,6], Marcus B. Foston[5], Hugh O'Neill[1], Volker S. Urban[1], Arthur Ragauskas[2,4], Barbara R. Evans[3], Brian H. Davison[2] and Sai Venkatesh Pingali[1*]

[1]Neutron Scattering Division, [2]Biosciences Division, [3]Chemical Sciences Division, Oak Ridge National Laboratory, Oak Ridge Tennessee 37831

[4]Department of Chemical and Biomolecular Engineering, University of Tennessee, Knoxville, Tennessee 37996

[5]Department of Energy, Environmental and Chemical Engineering, Washington University in St. Louis, St. Louis, Missouri 63130

[6]Present address: School of Food and Advanced Technology, Massey University, Auckland 0632, New Zealand

This manuscript has been authored by UT-Battelle, LLC, under Contract No. DE-AC05-00OR22725 with the U.S. Department of Energy. The United States Government retains and the publisher, by accepting the article for publication, acknowledges that the United States Government retains a non-exclusive, paid-up, irrevocable, world-wide license to publish or reproduce the published form of this manuscript, or allow others to do so, for United States Government purposes. The Department of Energy will provide public access to these results of federally sponsored research in accordance with the DOE Public Access Plan (http://energy.gov/downloads/doe-public-access-plan).

*Corresponding author: Sai Venkatesh Pingali

E-mail: pingalis@ornl.gov

Keywords: Switchgrass; Small-angle neutron scattering; Dilute acid pretreatment; Lignin aggregation; Hemicellulose aggregation

Abstract

Production of second-generation bioethanol from lignocellulosic biomass requires pretreatment to open the plant cell wall structure and improve enzyme access. Many different thermochemical pretreatments have been extensively developed and employed, but the exact nature of plant cell wall recalcitrance and the most efficient and economical approach to alter plant cell wall structure via pretreatment still remains elusive. In order to understand the role of non-cellulosic switchgrass polymers on the overall efficiency of pretreatment, the structural evolution of the non-cellulosic polymers of the plant cell wall were investigated during dilute acid pretreatment (DAP) by employing *in-situ* small-angle neutron scattering (*in-situ* SANS). In this study, we observed real-time structural changes not possible to observe by any other technique. To deconvolute the structural evolution of lignin and hemicellulose polymers during DAP, native switchgrass (NATV), isolated holocellulose (HOLO), and cellulose (CELL) fraction from NATV were studied. Our results show aggregate particles first appear around 80 °C for NATV and HOLO samples. Due to the low temperature and low pretreatment severity condition, these particles are likely derived from hemicellulose. The formation of much larger aggregate particles, only observed in the NATV sample, were attributed to lignin. For the HOLO sample, as the temperature and pretreatment severity condition increased hemicellulose-derived aggregate particle sizes also increased suggesting maybe the nucleation and early-stage formation of pseudo-lignin particles. Consistent with our interpretation of structural evolutions in NATV and HOLO samples, no formation of aggregate particles was observed in CELL samples for the entire duration of the pretreatment. These results suggest that not only lignin, but also hemicellulose can form aggregate particles within plant cell walls during pretreatment affecting pretreatment efficacy.

Introduction

The plant cell wall exhibits a complicated and hierarchical structure; carbohydrate polymers, mainly cellulose and hemicellulose, interact with each other and the hydrophobic polymer, lignin, provides structural integrity to the plant.[1] During the production of biofuels, which involves enzymatic depolymerization of carbohydrate polymers into fermentable sugars, various enzymes need to access and hydrolyze the carbohydrate polymers.[2] However, the structure of the plant cell wall is naturally

designed to resist attack by bacterial and fungal enzymes, so the enzymes find it difficult to access the carbohydrate polymers. Therefore, it is necessary to develop approaches to increase enzyme access to the plant cell to make biological approaches to biofuel production economical. To achieve improved enzyme access, thermochemical pretreatments are employed to alter and deconstruct the cell wall structure prior to enzymatic depolymerization.[3] Among the various pretreatment strategies, dilute sulfuric acid pretreatment (DAP) associated with a high temperature and short residence time treatment has been considered as the most promising approach because of its ease of application and low-cost. The characteristics of DAP, dilute aqueous sulfuric acid (1-2%) and short residence time prevents formation of sugar degradation products which can additionally inhibit enzymatic activity and yeast growth.[4, 5] Despite the widespread use of DAP, the fundamental understanding of the exact effect of DAP on the structure of the different plant cell wall polymers is still elusive.[6-8]

In recent years, we have employed small-angle neutron scattering (SANS) to study the multi-scale structural changes of various biomass samples during different pretreatments both *in-situ* and *ex-situ* covering multiple length scales from several nanometers to hundreds of nanometers.[5-8] The high penetrating power and non-destructive nature of neutrons make SANS an attractive technique for biomass structural characterization, in particular, to perform real-time structural analysis during pretreatments. For instance, *in-situ* SANS studied morphological changes in the cellulose and lignin components of quaking aspen (*Populus tremuloides*) during steam pretreatment at 180 °C and found-cellulose microfibril coalesces in the reactor heating phase, lignin aggregate nucleation occurs at the target pretreatment temperature at the start of the reactor holding phase, and those lignin aggregates grow in size upon the completion of the reactor holding and cooling phases.[7] In other studies SANS was utilized to investigate the multiscale structural changes of switchgrass and poplar during DAP and demonstrated that both biomass materials undergo coalescence of elementary cellulose fibrils and lignin aggregate formation during the treatment.[6, 8] The common results in these SANS studies, support and provide early stage evidence of cellulose crystallinity increase, cellulose crystallite size increase, and lignin droplet formation observed as a result of hydrothermal pretreatment methods. [9-13]

Ex-situ SANS measurements of reaction provided a rough estimate of the temperature when lignin aggregation is initiated: ~150 °C.[8] In an effort to improve our understanding of the changes that occur

to the morphology and structure of biomass during pretreatment and deconvolute the effect of pretreatment reactor heating, holding, and cooling phases, SANS measurements were performed in real-time. This real-time mode of measurement allows us to probe transient changes that would otherwise be lost. For example, how the presence of hemicellulose and lignin amorphous polymers alter the deconstruction process or how hemicellulose influences the structural evolution of lignin. Besides lignin, the structural evolution of hemicellulose is also critical. Recent studies show that hemicellulose can precipitate and re-associate with cellulose during the DAP, which increases cellulose recalcitrance to biological conversion, especially at commercially viable low enzyme loadings.[8,14] In this manuscript, *in-situ* SANS[6, 8] was used to probe the structural changes of hemicellulose and lignin with native switchgrass (NATV), extracted holocellulose (HOL) and extracted cellulose (CEL) during DAP.

Materials and Methods

Native switchgrass sample

Lowland cultivar Alamo switchgrass (*Panicum* V*irgatum*), harvested at Oak Ridge National Laboratory, TN were shipped to the National Renewable Energy Laboratory (NREL) in Golden, CO, for room temperature air-drying and Willy mill size-reduction (20-mesh screen particle size). These were used as samples and stored in a freezer to maintain the moisture content. The monosaccharide and lignin content of the untreated and lignin extracted switchgrass samples was determined by employing previously described standard procedures and the results summarized in Table 1 have already been published[6].

Table 1. Compositions of the native and component-extracted switchgrass[6, 8]

Samples[+]	arabinose	galactose	glucose	xylose	mannose	lignin
NATV	2.93	1.66	43.06	20.84	0.34	31.18
HOLO	4.75	1.62	57.01	30.23	0.00	6.40

The numbers are shown in mass percentages (% (w/w)).
[+]CELL– monosaccharide composition was not assessed, but a well-established method for generating cellulose both for commercial and analytical purposes was employed.

Preparation of component-extracted switchgrass samples

Holocellulose and cellulose samples were prepared according to the methods described in the literature.[15] Briefly, in order to obtain extracted holocellulose (HOLO; lignin removed) from switchgrass, air-dried and milled switchgrass (~1.5 g) was suspended in 125 mL of deionized water in a Kapak sealing pouch. The samples were retained in a water bath controlled at 75 °C for 1 h before adding 1.0 mL of glacial acetic acid and 1.00 g of sodium chlorite ($NaClO_2$) and proceeding the pretreatment for another 1 h. This procedure was repeated for 3 times up to 3 h to ensure complete removal of lignin. The treatment was stopped by quenching the mixtures in ice-water and filtered. To obtain the HOLO sample, the acid-chlorite pulped switchgrass was thoroughly washed with deionized water followed by acetone rinse and finally air-dry overnight. The extracted cellulose (CELL; lignin and hemicellulose removed) was obtained by treating HOLO further with 2.5 M hydrochloric acid at 100 °C for 4 h. The resulting samples were thoroughly rinsed with deionized water to remove the solubilized hemicellulose. Finally, the samples were rinsed with acetone and air-dried. Note that the current procedures used to remove lignin and hemicellulose have been shown to have minimal effect on the hemicellulose and cellulose structure. [16]

Small-Angle Neutron Scattering

In-situ small-angle neutron scattering (*in-situ* SANS) measurements were conducted on the CG-3 Bio-SANS instrument at the High Flux Isotope Reactor (HFIR) facility of Oak Ridge National Laboratory (ORNL).[17, 18] Two different instrument configurations were employed to measure data over the total range of scattering vectors, $0.0045 < Q\ (Å^{-1}) < 0.3$, by employing sample-to-detector distances of 2606 and 10906 mm and 6 Å neutron wavelength, λ. In each configuration, the center of the area detector (Ordela 2410N) was offset by 150 mm from the beam. The instrument resolution was defined by the placement of two circular apertures of diameters 40 mm (source) and 10 mm (sample) at distances of 2966 mm and 11066 mm, respectively. The Q-range offered by these two configurations were $0.018 < Q\ (Å^{-1}) < 0.3$ for the short configuration and $0.0045 < Q\ (Å^{-1}) < 0.03$ for the long configuration. The relative wavelength spread $\Delta\lambda/\lambda$ was set to 0.15. The processed 2D images were normalized to incident beam monitor counts, corrected for detector dark current, pixel sensitivity, and solvent scattering backgrounds (quartz cell filled with D_2O solvent). Subsequently, the processed 2D images were azimuthally averaged to generate scattering intensity profiles $I(Q)$ versus Q. All samples (NATV, HOLO, and CELL) were soaked in 100% D_2O solvent for at least 24 h during which the solvent was replaced with a fresh 100% D_2O solvent 2-3 times to achieve maximum solvent

penetration and D/H exchange. The soaked samples, while still wet, were immersed into 1.0 v/v % sulfuric acid-D_2O solvent and loaded into a pressure cell. The pressure cell was modified to execute the industrial protocol of dilute acid pretreatment to breakdown biomass (see 'Reaction Cell for *in-situ* SANS' section for details). The soaked biomass particulates were positioned within the cell to ensure neutron beam penetrates the sample. *In-situ* SANS data series were collected in 1 min exposures to monitor in real time the structural changes to biomass. The pretreatment reactions were repeated to collect reaction data in the two configurations; the temperature vs. time profile of the individual pretreatments were used to combine profiles with the same reaction time/temperature from the two reactions to obtain a single SANS profile.

Reaction Cell for in-situ SANS

The reaction cell used to perform *in-situ* small-angle neutron scattering experiment is shown in Figure 1. The sample, visible through transparent windows, is sandwiched in the central core of the cylindrical cell body by sapphire crystal windows (Figure 1A). Each window is sealed by two chemically resistant Kalrez O-rings (i.e., each pretreatment uses four in total). The central body of the cell is held together by titanium caps fastened to the cell body. The thickness of the sample is defined by using a notch thickness in the center of the hollow cylindrical sleeve; a notch of 1 mm thickness was used for these experiments (Figure 1B). All parts of the cell that was determined to come in contact with the acidic solvent during pretreatment was subjected to the Tantaline® process which alloys Tantalum to stainless steel surfaces to render the cell resistant to corrosion in acidic environments. Four heating cartridges inserted into slots in the cell were used for heating the cell to a maximum temperature of 200 °C. Temperature during reaction was measured using a thermocouple inserted into the cell with the tip located close to the sample. The tunnel design limited the maximum accessible Q with this reaction cell to 0.2 $Å^{-1}$.

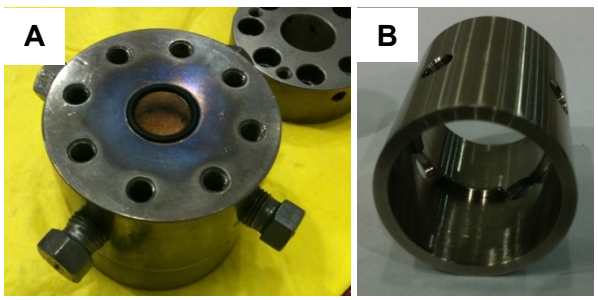

Figure 1. First-generation reaction cell used to perform *in-situ* small-angle neutron scattering studies. (A) The brownish particulates visible through sapphire crystals is the initial state of raw switchgrass (NATV) sample prior to dilute acid treatment. (B) The notch thickness in the center of the hollow cylindrical sleeve defines the sample thickness (1 mm).

The pretreatment protocol employed for DAP of biomass followed a modification of a previously reported procedure.[6, 19] A 1.0 vol% dilute sulfuric acid and approximately 10 wt% of biomass loading were used for these studies. *In-situ* SANS experiments recorded SANS profiles during the (1) reactor heating phase where the temperature of the sample was ramped up from room temperature to 180 °C at a rate of 5 °C/min, (2) reactor holding phase where the temperature of the sample was maintained at 180 °C for 60 min, and (3) reactor cooling phase where the temperature of the sample was reduced in an uncontrolled fashion to 50 °C within 15 min (see Figure 4A). Each *in-situ* SANS experiments took 2 h to complete.

SANS data analysis

SANS data, $I(Q)$ vs. Q, was analyzed using the Unified Fit routine implemented in the Irena SAS package that is embedded in the commercial Igor Pro software (Wavemetrics, USA). The Unified Fit model was utilized to deconvolute the contributions from the exponential and the power-law behaviors at each structural level and obtain the particle size, bulk and surface characteristics. The Unified Fit equation is [20, 21],

$$I(q) = \sum_{i=1}^{n} G_{\mathrm{i}} \exp\left(\frac{-q^2 R_{g_i}^2}{3}\right) + B_{\mathrm{i}} \exp\left(\frac{-q^2 R_{g_{i+1}}^2}{3}\right) \left[\frac{\left(\mathrm{erf}\left(\frac{qR_{g_i}}{\sqrt{6}}\right)\right)^3}{q}\right]^{P_i} \qquad (1)$$

where n is the number of structural levels used in the fit (n = 2 for all our fits with level-1 for high-Q and level-2 for low-Q region); G_i is the scalar for the Guinier component for the i^{th} level; R_{g_i} is the radius of gyration for the i^{th} level; B_i and P_i are the scalar and exponent of the power-law component for the i^{th} level, respectively. The Unified Fit has now been employed to analyze SANS scattering data of hierarchical biological systems, such as the bacterial cellulose-hemicellulose composites[22], switchgrass[6], and poplar[8] under different thermochemical pretreatment conditions.

Results and Discussion

Biomass deconstruction was investigated in real-time during DAP using an *in-situ* SANS reaction cell (see Figure 1). The SANS scattering profiles for NATV (Figure 2A), HOLO (Figure 2B), and CELL (Figure 2C) are plotted as a function of residence time. The scattering profiles were vertically shifted for clarity. For all the samples, there are two main structural regimes identified as high-Q, $0.02 < Q$ (Å^{-1}) < 0.16, and low-Q, $0.004 < Q$ (Å^{-1}) < 0.02 and each region (high- and low-Q) is modeled by a single level of the Unified Fit. The solid black lines in Figure 2 are the Unified Fits. The deconvoluted profiles for each individual level of the overall Unified Fit is shown in Figure 3. Each level consists of an exponential and a power-law function combined together as a single function (see 'SANS Data Analysis' section for details). The length scales covered by the high- and low-Q regions together range from 40 to 1600 Å.

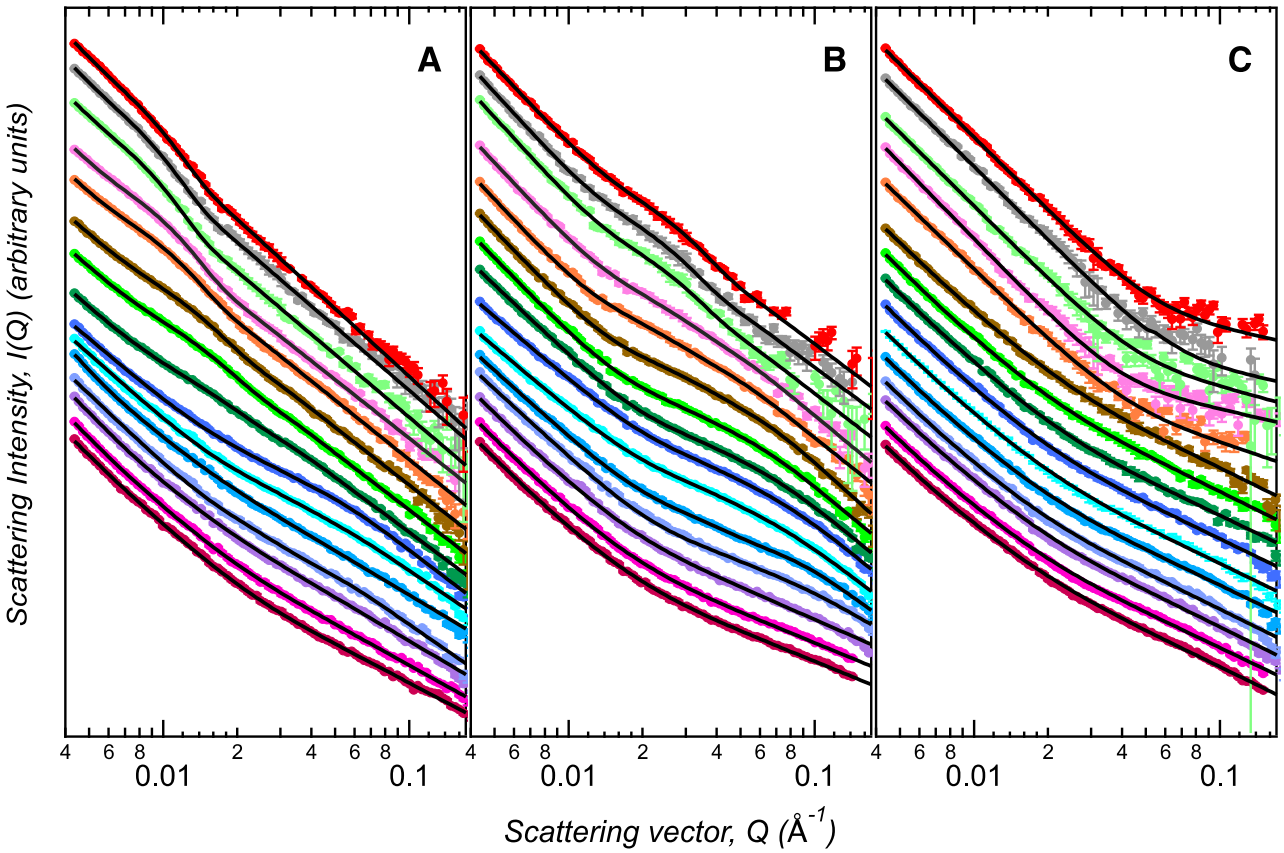

Figure 2. SANS curves of dilute acid pretreated (A) raw switchgrass (NATV), (B) switchgrass holocellulose (HOLO), and (C) switchgrass cellulose (CELL). The curves from bottom represent room temperature (~ 25 °C), and treated to approximately 50, 70, 80, 100, 120, 130, 150, 170 °C; retained at 180 °C for 1, 5, 15, 45, and 60 min; and cooling down to 50 °C. The exact temperatures

are listed in Tables S1-S3 (see supporting information). The Unified fits to the experimental SANS data are demonstrated as solid black lines. All the scattering curves are vertically shifted for clarity.

The fitting parameters consists of either (a) two power-law exponents, P_1 and P_2, one from each high and low-Q regions (Figure 3A) or (b) two power-law exponents, P_1 and P_2, and a radius of gyration, R_g sandwiched by the two power-law features (Figure 3B). In the former case, two straight lines (in a log-log plot) with different slopes intersect. The Q-value at which these slopes intersect is referred to as Q_c (Figure 3A) and is related to the cross-over R_g (Table 2). This parameter, cross-over R_g represents transition from local, individual polymer chain conformation (P_1) to bulk polymer organization (P_2). In the latter case, a particle size feature indicated by the arrow in Figure 3B is related to the high-Q R_g parameter. The fitting parameters of the Unified Fit for the two examples are summarized in Table 2. This fitting strategy was applied to all the SANS profiles and the trend in these fitting parameters as a function of residence time is shown in Figure 4 and the fit parameter values with σ_1 error bar is listed in Tables S1-S3 for samples NATV, HOLO, and CELL, respectively.

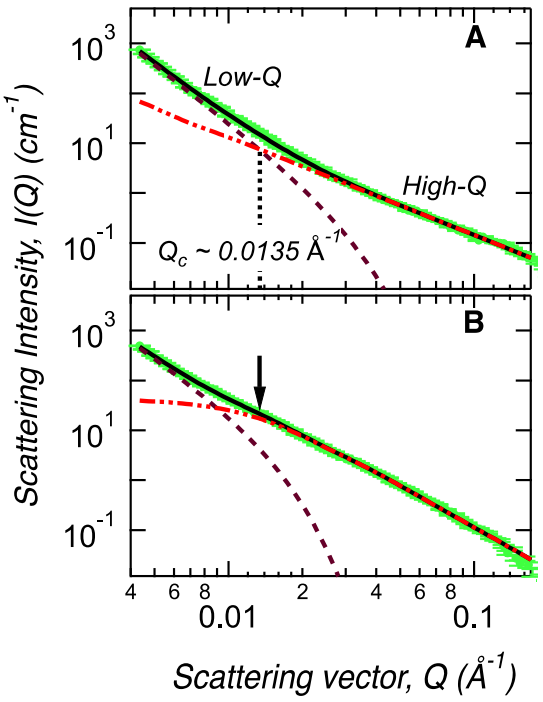

Figure 3. SANS data of (A) native raw switchgrass (NATV) at room temperature and (B) dilute acid treated to 150 °C. The Unified fits to the experimental SANS data are demonstrated as solid black

lines and individual levels are illustrated as red and brown dashed lines for high-Q (level-1) and low-Q (level-2), respectively. The arrow in panel-B represents a particle scattering feature in the high-Q fitting region.

Table 2. Unified fit structural parameters of native raw switchgrass at room temperature and dilute acid treated to 150 °C.

Time (*min*)	Temp. (° *C*)	High-Q Guinier		High-Q Power-law		Low-Q Power-law		Cross-over R_g (Å)[#]
		Scalar, G (cm^{-1})	Size, R_g (Å)	Scalar, B (x 10^{-4})	Exponent, P	Scalar, B (x 10^{-6})	Exponent, P	
1	25.6	–	–	12 (2)	2.0 (0.1)	0.4 (0.1)	3.8 (0.1)	64 (3)
26.5	150.4	60 (13)	150 (13)	1.7 (0.3)	2.8 (0.1)	7.0 (2.0)	3.4 (0.1)	

Numbers in parentheses represent σ error bars (or 68% confidence levels)
[#]The cross-over R_g is related to Q as $R_g \sim Q_c^{-1}$, where Q_c is the intersection between the high- and low-Q power-law slopes

The power-law exponents for the high-Q region are shown below the dashed line (P = 3) while the power-law exponents above the dashed line are for the low-Q region (Figure 4D). During the reactor heating phase of DAP for the NATV sample, 80 °C onwards, the onset of a shoulder feature (arrow in Figure 3B) in the high-Q region shows the presence of particles (also see Figure S1 for comparison of 25 and 80 °C profiles). These particles are also referred to as globules [23] or droplets [9]. The observed exponent of 2.6 in the high-Q region for 81.1 °C (see Table S1) implies that the polymers in the NATV aggregate particles are intertwined (or branched). As the temperature is further increased to 130 °C the exponent approaches 3.0 indicating that the polymers in the aggregate particles have become highly dehydrated and collapsed, forming a highly interconnected network.[21, 24] For those temperature curves that do not show a particle formation for NATV samples (i.e., below 80 °C), the high-Q exponent represents local organization of the polymers within the cell wall.[6] The exponent is 2.1 indicating a flexible polymer conformation for length scales below 130 Å.

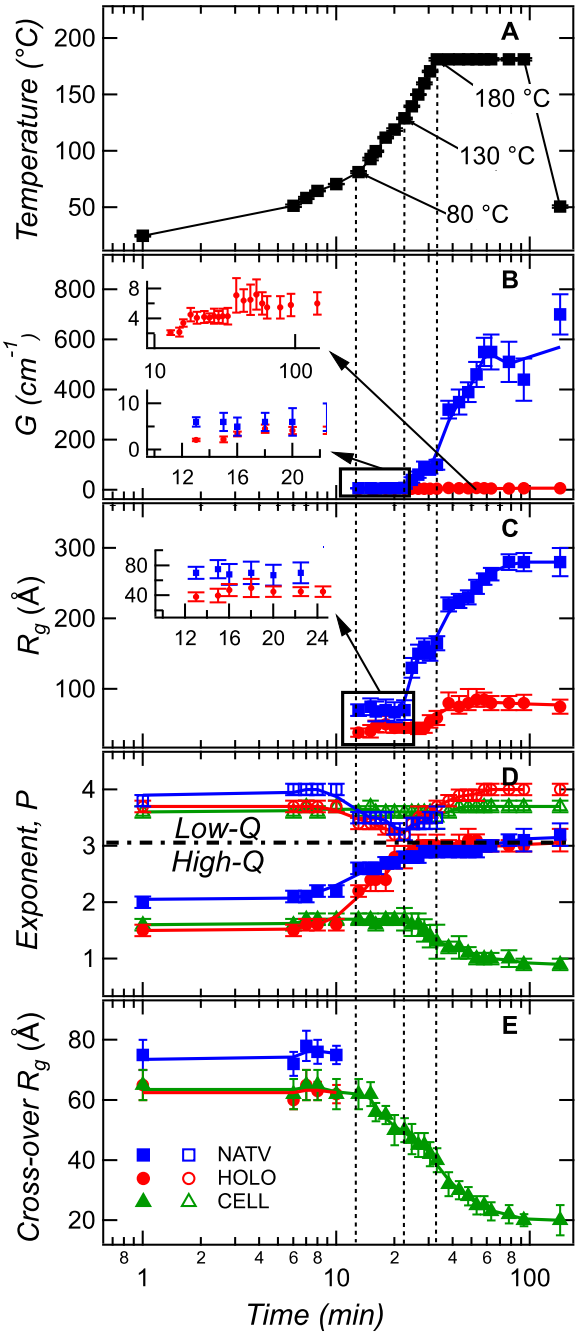

Figure 4. As a function of reaction time, the plot summarizes the profiles of raw switchgrass (NATV), extracted switchgrass holocellulose (HOLO), and extracted switchgrass cellulose (CELL) for (A) reaction temperature, and the trends for Unified fit parameters for (B) particle size scalar, *G*, (C) radius of gyration of particle, R_g, (D) power-law exponent, *P* for high-*Q* region (*High-Q*), and low-*Q* region (*Low-Q*) and (E) cross-over R_g. The solid lines are meant to guide the eye in the trends. Two insets in panel-B provides clarity to particle size scalar G for HOLO sample and initial reaction time points within the box for both samples. Similarly, the inset in panel-C expands the details in the initial reaction time points within the box for both samples.

The low-Q power-law exponent for NATV sample at 25 °C is 3.8 (Figure 4D). A power-law exponent of 3.8 represent a nearly smooth surface since, a smooth surface exhibits an exponent of 4.0 and a highly rough surface, 3.0. As the target pretreatment temperature of 180 °C was reached, the low-Q exponent decreased to ~3.5 implying that the cell wall surfaces became progressively rougher. After several minutes of residence at 180 °C, the aggregate particles continued to grow in size resulting in the particle size feature shifting to lower-Q values in the scattering profile. Consequently, the available Q-range in the low-Q region progressively reduced and the power-law fit in the low-Q region was no more reliable to extract a robust power-law exponent. Therefore, the low-Q exponent from 38 min at 180 °C (hold phase) was fixed at an exponent of 4.0. The choice to fix the exponent to 4.0 was based on the results observed for HOLO sample and discussed below.

During the reactor heating phase, an average particle size, R_g of ~70 Å (Figure 4C inset) appears as the pretreatment reaches 80 °C and remains constant until 130 °C. However, from 130 to 180 °C, a sharp increase in the particle size is observed, from 70 to 165 Å (i.e., the particle size doubles in about 10 min). During the first 45 min of the reaction holding phase, these particles increase from 165 to 280 Å. For the remainder of the reactor holding phase the particle size continues to increase at a deaccelerating rate.

The scalar parameter (G) of these aggregate particles (Figure 4B) for the NATV sample remained relatively constant, from 80 to 130 °C, at ~ 6 cm^{-1} (Figure 4B below inset) followed by a dramatic increase in particle size above 130 °C to ~ 700 cm^{-1}. The scalar parameter is proportional to the aggregate average particle volume ($V \sim R_g^3$), particle-solvent contrast, and particle number concentration (C). Assuming a constant aggregate particle-solvent contrast during reaction, the scalar parameter ($G \sim V^2C$) can be reduced to be proportional to the particle volume and concentration. In an effort to display trends, normalized scalar parameter ($G/G_{80\ ^\circ C}$), normalized average aggregate particle volume ($V/V_{80\ ^\circ C}$), and normalized aggregate particle concentration ($C/C_{80\ ^\circ C}$) have been presented in Table S4. Thus, the ratios in Table S4 describe the change in scalar parameter, average aggregate particle volume, and aggregate particle concentration compared to that observed at 80 °C when aggregates first appear. Since the aggregate particle concentration decreases with pretreatment, the normalized scalar parameter suggests that the total volume occupied by all scattering particles ($G \sim VC$) increased by a factor of ~1.8 times that observed at 80 °C and that a significant fraction of

the non-cellulosic cell wall polymers observed as well-dispersed, flexible polymer conformations < 80 °C, are converted into aggregate particles. Normalized average particle volume values show that the onset of particle growth during the reactor heating phase occurs at ~130 °C and that the resulting particle growth after pretreatment resulted in particles with an average volume ~60 times larger than the particles that first appeared.

Similar to NATV, HOLO samples too show the appearance of aggregate particles. These aggregates also appear during the pretreatment reactor heating phase once the reaction has reached 80 °C (Figure 4C). The average particle size (R_g) between particle appearance at 80 °C and near the end of heating phase at 170 °C remain unchanged at 45 Å. The onset temperature for aggregate particle growth of the HOLO sample, ~170 °C, is much higher than that observed for NATV sample, which was ~130 °C. Particle growth increased the particle R_g to 80 Å as the pretreatment target temperature of 180 °C was attained. No further change in aggregate particle size was observed until completion of pretreatment. Employing the same calculations performed for NATV, normalized scalar parameter, normalized average aggregate particle volume, and normalized aggregate particle concentration were performed for HOLO and shown in Table S5. The normalized scalar parameter increased only by a factor of 3 over the course of the entire pretreatment suggesting only a minor fraction of the non-cellulosic cell wall are converted into aggregate particles during pretreatment. Normalized average particle volume values show an onset of particle growth during the reactor heating phase between 100-130 °C, a plateauing of particle growth, and then another onset of particle growth at 180 °C at the start of the reactor holding phase. The particles found after pretreatment had an average volume 8-10 times larger than the particles that first appear.

Comparing the high-Q power-law exponents from 80 °C (Figure 4D), HOLO particles show a slightly lower exponent of 2.2 than 2.6 for NATV. This implies that the polymers in the HOLO aggregate particles are less entangled than the NATV aggregate particles. As the temperature was increased to 130 °C, the exponent increased to 3.0 displaying a similar behavior to that observed for NATV; the aggregate particles progressively dehydrate (or collapse) and become highly interconnected.[21, 24] For curves that do not show a particle feature (i.e., below 80 °C), the exponent was 1.5 for the HOLO sample which indicates a semi-rigid polymer conformation.[25] The dramatic reduction in the content of lignin molecules in HOLO sample compared to NATV sample has significantly reduced the power-

law exponent indicating a shift from a random polymer conformation for NATV to a semi-rigid polymer conformation for HOLO. In fact, all the curves of CELL sample show a similar exponent of 1.5-1.7 below 160 °C as observed for HOLO sample curves below 80 °C; and the exponent further reduced to 1.3 by increasing temperature to 180 °C. This trend suggests that the skeleton cellulose microfibril structure in CELL sample at 180 °C has a reduced degree of flexibility and progressively becomes more rigid rod-like. Another important feature is the cross-over R_g, i.e., the inverse of the Q value at which the high- and low-Q power-law slopes intersect. The cross-over R_g for CELL reduced from 55 to 20 Å over the pretreatment suggesting that the large structures such as the macrofibrils (i.e., microfibril bundles) or the cell wall lumens progressively break down by the dissociation of small structures that contribute to the transition of the slope-intersection to higher-Q values (Figure 4E).

Prior to the start of pretreatment, at 25 °C, the low-Q power-law exponent for NATV sample was 3.8 and the sequential removal of lignin (in HOLO) and then of hemicellulose (in CELL), shows a progressive transition to rougher surfaces reflected by the decrease of the exponent, to 3.7 and 3.6, respectively (Figure 4D). As the pretreatment temperature reached 180 °C, the low-Q exponent for CELL sample changed minimally from 3.6 to 3.5 consistent with a sample that has almost no amorphous polymers (lignin/hemicellulose) to potentially smooth the surfaces by filling the surface crevices. In comparison, the low-Q exponent of HOLO sample, like NATV, decreased to ~3.5 implying that the surface of the large structures in all these samples match that of pure cellulose, CELL sample. On further progression of the pretreatment, the cell wall surface morphology transitioned back to an exponent of 4.0 for HOLO suggesting a transition to smooth surface morphology of the large cellulose structures rendered by the redeposition of hemicellulose amorphous polymer. Since, NATV sample consists of both lignin and hemicellulose, like in HOLO sample, these amorphous polymers too will redeposit to smoothen the surfaces of the large structures at long reaction times. As a result, the low-Q exponent for NATV sample was fixed at 4.0 for curves collected at long pretreatment times, especially for temperatures point where the low-Q region available for fit was significantly reduced.

In this study, the hierarchical morphology and structural changes elucidated from the *in-situ* SANS measurement of NATV, HOLO, and CELL samples during DAP were (1) aggregate particle

formation and growth by the non-cellulosic plant polymers; (2) molecular arrangement in the aggregate particles; and (3) cellulose microfibril bundle or cell lumen surface morphology.

Aggregate particle formation and growth by the non-cellulosic plant polymers

The evolution of the aggregate particle size during pretreatment significantly differs between NATV and HOLO samples. NATV shows three distinct aggregate particle growth phases, during the: heating phase between 80-130 °C, heating phase between 130-180 °C, and holding phase for 60 min at 180 °C. Although not as distinct as NATV, HOLO particle growth can be segregated into three phases: heating phase between 80-170 °C, heating phase between 170-180 °C, and holding phase for 60 min at 180 °C. Compositional studies[6, 8] for these samples determined NATV sample has 30 wt% Klason lignin and 25 wt% hemicellulose, while HOLO sample has 6 wt% Klason lignin and 35 wt% hemicellulose. Our *ex-situ* and *in-situ* SANS studies[6,8] suggest the aggregate particles found at the end of the pretreatment of the NATV sample are attributed to lignin and coarsely confirm the temperature of lignin-derived aggregate formation at ~150 °C . Using electron microscopy, corn stover and hardwood chips were shown to have 5 nm to 10 μm diameter droplets on the cell wall surface after hydrothermal pretreatment, attributing the droplet composition and formation to lignin.[10] We, along with others, suggest the major mechanism for lignin aggregate particle or droplet formation is lignin thermal transition from a glass to rubbery states, migration of lignin due to rubbery flow, coalescence of lignin to minimize surface energy in aqueous media, and extrusion of the lignin into droplets on the cell wall surface. [9] For this to occur, the pretreatment must be above the glass transition temperature range (110–180 °C)[26-28] of lignin. In the NATV sample, there is the significant onset of particle growth above 130 °C suggesting the particles associated with significant increases in normalized scalar parameter and average particle volume are related to lignin. However, particles in this study, for both NATV and HOLO samples, show particle formation at 80 °C which is well below the lignin glass transition temperature range. Thus, the discussion below explores the possible origins of aggregate particles observed between 80-130 °C.

The formation of particles, as a result of pretreatment, originate from cell wall matrix polymers (i.e., hemicellulose and/or lignin) cycling between solid and liquid phases, leading to particle nucleation and growth, through: (1) thermal transition and motion; (2) depolymerization, diffusion of soluble fragments, and repolymerization; and/or (3) solubilization, diffusion of soluble polymers, and

precipitation. [9, 29] Although the HOLO sample had been pulped, there is still 6 wt% lignin content remaining. Therefore, we must consider two possible scenarios, where aggregate particles observed between 80-130 °C are derived from lignin in one case or hemicellulose in another. The aggregate particles observed between 80-130 °C in the HOLO sample are smaller and less abundant that those in the NATV sample. This fact is consistent with the HOLO sample having a lower lignin content than the NATV sample and having aggregate particle nucleation and growth limited by a lignin content reduced by a factor of 5. However, if aggregate particles observed in HOLO and NATV samples between 80-130 °C were derived from lignin, some lignin solid-liquid cycling pathway would have to occur in dilute aqueous acid at or below 80 °C, which is unlikely with what is known about lignin. The more probable scenario involves the nucleation and growth of particles derived from hemicellulose.

Hemicelluloses with specific monomeric compositions[30] have been reported to remain undissolved in aqueous solvents and exhibit recalcitrant behavior such as enhanced affinity to cellulose when subjected to DAP[31]. DAP-treated switchgrass and birchwood hemicellulose have also been shown to form oligomers[32, 33] and SANS have been used to characterize the oligomeric structures formed by hemicellulose.[34, 35] These hemicellulose behavioral characteristics suggest particle formation at 80 °C is possible. Consistent with this interpretation, the formation of these particles was not observed in CELL sample which is expected as there is no hemicellulose and lignin in the CELL sample.

The aggregate particles in the NATV sample begin to grow between 130-170 °C which is not observed on a significant level for the HOLO sample. During this phase in the NATV sample, either hemicellulose-derived aggregate particles continue to grow, presumably from lignin addition, or a separate distribution of lignin-derived aggregate particles form that increases the average particle size distribution with respect to that observed for the HOLO sample. The significant increase in the scalar parameter during this phase for the NATV sample suggest the latter is more probable. The average volume of aggregate particles in HOLO between 170-180 °C increases and then remains fairly unchanged for the reminder of the pretreatment. Pseudo-lignin, characterized by the formation of spherical droplets that contain a combination of carbohydrate and lignin degradation products, has been shown to form as a result of DAP and suggested to have a significant inhibitory effect on enzymatic hydrolysis. Pseudo-lignin formation has been observed in pretreated poplar holocellulose

at a combined pretreatment severity as low as 2.97.[36] Combined severity, CS is defined as $CS = log\left[t \times exp\left((T - T_{ref})/14.7\right)\right] - pH$, where t is the residence time (min) at the pretreatment temperature, T (°C) and T_{ref} is the reference temperature of 100 °C and pH is the pH (=1.0) of the acidic solvent (0.1 M H_2SO_4 aqueous solvent). The *in-situ* SANS experiment on the HOLO sample in this study, the pretreatment CS is 2.5 and 3.1 at 10 and 60 min into holding phase. Thus, we propose the aggregate particles observed in the HOLO samples are evidence of an early stage of pseudo-lignin droplet formation. The aggregate particles in the NATV sample observed in the heating phase between 130-180 °C and holding phase for 60 min at 180 °C are attributed primarily to processes of lignin. However, we suspect similar processes occurring in the HOLO sample also happen in the NATV sample.

Molecular arrangement in the aggregate particles

As the aggregate particles first appear, solvent penetrates the aggregates, resolving the conformational organization of polymers within. The bulk morphology of the aggregate particles upon their appearance at 80 °C indicates an amorphous morphology with a low degree of entanglement. Most probably, these aggregate particles are derived predominantly of hemicellulose. However, the degree of entanglement is slightly higher for NATV sample compared to HOLO sample, suggesting the NATV sample aggregate particles maybe derived from a mix of lignin and hemicellulose.[37] With increasing temperature as aggregate particles are formed in NATV sample, derived primarily of lignin, the polymer morphology in these aggregate particles progressively become more dehydrated and highly interconnected ($P_1 \sim 3.0$).

Cellulose microfibril bundle or Cell lumen surface morphology

Although the maximum dimension of the large particles (either cellulose microfibril bundles of R_g's up to 500 Å or the cell lumen of 20-40 μm) is not accessible, the surface characteristics are observed until $Q \sim 0.05$ Å^{-1} and the length scales (R_g) accessed are in the range of 62 Å ($Q_c \sim 0.016$) to 250 Å. For the native switchgrass plant, the surface morphology of these large structures that represent either cellulose microfibril bundle or cell lumen is smooth, i.e., the power-law exponent, P is ~4.0 [21]. The removal of lignin and hemicellulose disrupts this smooth morphology and makes the surface rougher (< 4.0). Lignin extraction causes the most change in the cell wall surface roughening while hemicellulose removal has a minimal effect. DAP has a similar effect on the surface morphology as

observed due to component extraction, only to a greater extent. The NATV sample undergoes a roughening that could be measured until the end of the heating phase and thereafter was not accessible. The surface morphology of HOLO sample showed an interesting trend. The surface characteristic of the HOLO sample initially transitioned to a rough surface during the heating phase as the pretreatment reached 120-130 °C. However, with further increase in temperature to 180 °C, the surface characteristic progressively becomes smooth and remained so throughout the remainder of the pretreatment. Coincidently, the temperatures for surface roughening and then smoothening behavior between 120-180 °C for the HOLO sample correlated well with the onset temperature of lignin glass transition temperature and pseudo-lignin formation. The CELL sample showed no change in the surface morphology throughout the entire pretreatment. This implies that surface morphology changes observed in the HOLO and NATV samples are related to hemicellulose and lignin extraction and re-deposition on cellulose microfibril bundle or cell lumen surfaces.

Conclusions

In-situ SANS measurements revealed time-resolved structural and morphological changes occurring to the hierarchical structure of the switchgrass cell wall during DAP deconvoluting the effect of the reactor heating, holding, and cooling phases. The NATV, HOLO, and CELL samples were subjected to the same treatment conditions and the resulting SANS analyses were integrated to develop a holistic understanding of the behavior of lignocellulosic cell wall during DAP. SANS analysis revealed that DAP induces aggregate formation around 80 °C for both NATV and HOLO samples which was associated to hemicellulose-derived aggregates. At a higher temperature range of 130-170 °C, larger-sized aggregates observed for only NATV samples was associated to lignin-derived aggregates. Further, surface morphology of the large particles possibly cellulose microfibril bundles or cell lumens became significantly rough. These results, for the first time, suggest hemicellulose aggregate particles form under mild hydrothermal conditions and under more severe pretreatment conditions could be the origins of pseudo-lignin droplets. Consequently, these hydrothermal pretreatments are less effective at the removal of hemicellulose from cell wall surfaces than bulk compositional analysis would indicate.

Acknowledgements

Switchgrass samples and cell wall compositional data were obtained through a collaborative agreement with the BioEnergy Science Center (BESC) funded by DOE Office of Science, Office of Biological and Environmental Research and located at the Oak Ridge National Laboratory, Oak Ridge, Tennessee. This research was funded by the DOE Office of Science, Office of Biological and Environmental Research under the Genomic Sciences Program (FWP ERKP752). Neutron scattering research conducted at the Bio-SANS instrument, a DOE Office of Science, Office of Biological and Environmental Research resource, used resources at the High Flux Isotope Reactor, a DOE Office of Science, Scientific User Facility operated by the Oak Ridge National Laboratory.

Oak Ridge National Laboratory is managed by UT-Battelle, LLC, for the U. S. Department of Energy under Contract DE-AC05-00OR22725. This manuscript has been authored by UT-Battelle, LLC, under Contract No. DE-AC05-00OR22725 with the U.S. Department of Energy. The United States Government retains and the publisher, by accepting the article for publication, acknowledges that the United States Government retains a non-exclusive, paid-up, irrevocable, world-wide license to publish or reproduce the published form of this manuscript, or allow others to do so, for United States Government purposes. The Department of Energy will provide public access to these results of federally sponsored research in accordance with the DOE Public Access Plan (http://energy.gov/downloads/doe-public-access-plan).

Supporting Information

The Supporting Information is available online free of charge.

- Tables of Unified fit parameters of raw switchgrass (NATV), extracted switchgrass holocellulose (HOLO), and extracted switchgrass cellulose (CELL) during dilute acid pretreatment.
- Tables of calculated particle concentrations from fit results of raw switchgrass (NATV) and extracted switchgrass holocellulose (HOLO).
- Figure of SANS data of raw switchgrass (NATV) 25° and 80°C during dilute acid pretreatment.

Notes

The authors declare no competing financial interest.

References

1. Foston, M.; Ragauskas, A. J., Biomass characterization: recent progress in understanding biomass recalcitrance. *Industrial Biotechnology* **2012,** *8* (4), 191-208. http://doi.org/10.1089/ind.2012.0015
2. Ragauskas, A. J.; Williams, C. K.; Davison, B. H.; Britovsek, G.; Cairney, J.; Eckert, C. A.; Frederick, W. J.; Hallett, J. P.; Leak, D. J.; Liotta, C. L., The path forward for biofuels and biomaterials. *Science* **2006,** *311* (5760), 484-489. http://dor.org/10.1126/science.1114736
3. Mood, S. H.; Golfeshan, A. H.; Tabatabaei, M.; Jouzani, G. S.; Najafi, G. H.; Gholami, M.; Ardjmand, M., Lignocellulosic biomass to bioethanol, a comprehensive review with a focus on pretreatment. *Renewable and Sustainable Energy Reviews* **2013,** *27*, 77-93. http://doi.org/10.1016/j.rser.2013.06.033
4. Nishiyama, Y.; Langan, P.; O'Neill, H.; Pingali, S. V.; Harton, S., Structural coarsening of aspen wood by hydrothermal pretreatment monitored by small-and wide-angle scattering of X-rays and neutrons on oriented specimens. *Cellulose* **2014,** *21* (2), 1015-1024. https://doi.org/10.1007/s10570-013-0069-2
5. Langan, P.; Petridis, L.; O'Neill, H. M.; Pingali, S. V.; Foston, M.; Nishiyama, Y.; Schulz, R.; Lindner, B.; Hanson, B. L.; Harton, S.; Heller, W. T.; Urban, V.; Evans, B. R.; Gnanakaran, S.; Ragauskas, A. J.; Smith, J. C.; Davison, B. H., Common processes drive the thermochemical pretreatment of lignocellulosic biomass. *Green Chemistry* **2014,** *16* (1), 63-68. https://doi.org/10.1039/C3GC41962B
6. Pingali, S. V.; Urban, V. S.; Heller, W. T.; McGaughey, J.; O'Neill, H.; Foston, M.; Myles, D. A.; Ragauskas, A.; Evans, B. R., Breakdown of cell wall nanostructure in dilute acid pretreated biomass. *Biomacromolecules* **2010,** *11* (9), 2329-2335. https://doi.org/10.1021/bm100455h
7. Pingali, S. V.; O'Neill, H. M.; Nishiyama, Y.; He, L.; Melnichenko, Y. B.; Urban, V.; Petridis, L.; Davison, B.; Langan, P., Morphological changes in the cellulose and lignin components of biomass occur at different stages during steam pretreatment. *Cellulose* **2014,** *21* (2), 873-878. https://doi.org/10.1007/s10570-013-0162-6
8. Pingali, S. V.; Urban, V. S.; Heller, W. T.; McGaughey, J.; O'Neill, H.; Foston, M. B.; Li, H.; Wyman, C. E.; Myles, D. A.; Langan, P., Understanding multiscale structural changes during dilute acid pretreatment of switchgrass and poplar. *ACS Sustainable Chemistry & Engineering* **2016,** *5* (1), 426-435. https://doi.org/10.1021/acssuschemeng.6b01803
9. Donohoe, B. S.; Decker, S. R.; Tucker, M. P.; Himmel, M. E.; Vinzant, T. B., Visualizing lignin coalescence and migration through maize cell walls following thermochemical pretreatment. *Biotechnology and Bioengineering* **2008,** *101* (5), 913-925. http://doi.org/10.1002/bit.21959
10. Selig, M. J.; Viamajala, S.; Decker, S. R.; Tucker, M. P.; Himmel, M. E.; Vinzant, T. B., Deposition of Lignin Droplets Produced During Dilute Acid Pretreatment of Maize Stems Retards Enzymatic Hydrolysis of Cellulose. *Biotechnology Progress* **2007,** *23* (6), 1333-1339. http://doi.org/10.1021/bp0702018
11. Sun, Q.; Foston, M.; Meng, X.; Sawada, D.; Pingali, S. V.; O'Neill, H. M.; Li, H.; Wyman, C. E.; Langan, P.; Ragauskas, A. J., Effect of lignin content on changes occurring in poplar cellulose ultrastructure during dilute acid pretreatment. *Biotechnology for Biofuels* **2014,** *7* (1), 1-14. https://doi.org/10.1186/s13068-014-0150-6
12. Samuel, R.; Pu, Y.; Foston, M.; Ragauskas, A. J., Solid-state NMR characterization of switchgrass cellulose after dilute acid pretreatment. *Biofuels* **2010,** *1* (1), 85-90. https://doi.org/10.4155/bfs.09.17
13. Foston, M.; Ragauskas, A. J., Changes in lignocellulosic supramolecular and ultrastructure during dilute acid pretreatment of Populus and switchgrass. *Biomass and Bioenergy* **2010,** *34* (12), 1885-1895. https://doi.org/10.1016/j.biombioe.2010.07.023
14. Jung, S.; Foston, M.; Sullards, M. C.; Ragauskas, A. J., Surface characterization of dilute acid pretreated Populus deltoides by ToF-SIMS. *Energy & Fuels* **2010,** *24* (2), 1347-1357. https://doi.org/10.1021/ef901062p
15. Foston, M.; Hubbell, C. A.; Davis, M.; Ragauskas, A. J., Variations in cellulosic ultrastructure of poplar. *BioEnergy Research* **2009,** *2* (4), 193. http://doi.org/10.1007/s12155-009-9050-1

16. Hubbell, C. A.; Ragauskas, A. J., Effect of acid-chlorite delignification on cellulose degree of polymerization. *Bioresource Technology* **2010,** *101* (19), 7410-7415. http://doi.org/10.1016/j.biortech.2010.04.029
17. Heller, W. T.; Urban, V. S.; Lynn, G. W.; Weiss, K. L.; O'Neill, H. M.; Pingali, S. V.; Qian, S.; Littrell, K. C.; Melnichenko, Y. B.; Buchanan, M. V., The Bio-SANS instrument at the high flux isotope reactor of Oak Ridge National Laboratory. *Journal of Applied Crystallography* **2014,** *47* (4), 1238-1246. https://doi.org/10.1107/S1600576714011285
18. Heller, W. T.; Cuneo, M.; Debeer-Schmitt, L.; Do, C.; He, L.; Heroux, L.; Littrell, K.; Pingali, S. V.; Qian, S.; Stanley, C., The suite of small-angle neutron scattering instruments at Oak Ridge National Laboratory. *Journal of Applied Crystallography* **2018,** *51* (2), 242-248. https://doi.org/10.1107/S1600576718001231
19. Samuel, R.; Pu, Y.; Raman, B.; Ragauskas, A. J., Structural characterization and comparison of switchgrass ball-milled lignin before and after dilute acid pretreatment. *Applied Biochemistry and Biotechnology* **2010,** *162* (1), 62-74. http://doi.org/10.1007/s12010-009-8749-y
20. Beaucage, Approximations leading to a unified exponential/power-law approach to small-angle scattering. *Journal of Applied Crystallography* **1995,** *28* (6), 717-728. https://doi.org/10.1107/S0021889895005292
21. Beaucage, G., Small-angle scattering from polymeric mass fractals of arbitrary mass-fractal dimension. *Journal of Applied Crystallography* **1996,** *29* (2), 134-146. https://doi.org/10.1107/S0021889895011605
22. Shah, R.; Huang, S.; Pingali, S. V.; Sawada, D.; Pu, Y.; Rodriguez, M.; Ragauskas, A. J.; Kim, S. H.; Evans, B. R.; Davison, B. H.; O'Neill, H., Hemicellulose–Cellulose Composites Reveal Differences in Cellulose Organization after Dilute Acid Pretreatment. *Biomacromolecules* **2019,** *20* (2), 893-903. https://doi.org/10.1021/acs.biomac.8b01511
23. Chundawat, S. P. S.; Donohoe, B. S.; da Costa Sousa, L.; Elder, T.; Agarwal, U. P.; Lu, F.; Ralph, J.; Himmel, M. E.; Balan, V.; Dale, B. E., Multi-scale visualization and characterization of lignocellulosic plant cell wall deconstruction during thermochemical pretreatment. *Energy & Environmental Science* **2011,** *4* (3), 973-984. https://doi.org/10.1039/C0EE00574F
24. Teixeira, J., Small-angle scattering by fractal systems. *Journal of Applied Crystallography* **1988,** *21* (6), 781-785. https://doi.org/10.1107/S0021889888000263
25. Pezron, I.; Djabourov, M.; Leblond, J., Conformation of gelatin chains in aqueous solutions: 1. A light and small-angle neutron scattering study. *Polymer* **1991,** *32* (17), 3201-3210. https://doi.org/10.1016/0032-3861(91)90143-7
26. Irvine, G., The significance of the glass transition of lignin in thermomechanical pulping. *Wood Science and Technology* **1985,** *19* (2), 139-149. https://doi.org/10.1007/BF00353074
27. Salmén, L., Viscoelastic properties ofin situ lignin under water-saturated conditions. *Journal of Materials Science* **1984,** *19* (9), 3090-3096. https://doi.org/10.1007/BF01026988
28. Shao, S.; Jin, Z.; Wen, G.; Iiyama, K., Thermo characteristics of steam-exploded bamboo (Phyllostachys pubescens) lignin. *Wood Science and Technology* **2009,** *43* (7-8), 643-652. http://doi.org/10.1007/s00226-009-0252-7
29. Trajano, H. L.; Engle, N. L.; Foston, M.; Ragauskas, A. J.; Tschaplinski, T. J.; Wyman, C. E., The fate of lignin during hydrothermal pretreatment. *Biotechnology for Biofuels* **2013,** *6* (1), 1-16. https://doi.org/10.1186/1754-6834-6-110
30. Shrestha, U. R.; Smith, S.; Pingali, S. V.; Yang, H.; Zahran, M.; Breunig, L.; Wilson, L. A.; Kowali, M.; Kubicki, J. D.; Cosgrove, D. J., Arabinose substitution effect on xylan rigidity and self-aggregation. *Cellulose* **2019,** *26* (4), 2267-2278. https://doi.org/10.1007/s10570-018-2202-8
31. Kumar, R.; Bhagia, S.; Smith, M. D.; Petridis, L.; Ong, R. G.; Cai, C. M.; Mittal, A.; Himmel, M. H.; Balan, V.; Dale, B. E., Cellulose–hemicellulose interactions at elevated temperatures increase cellulose recalcitrance to biological conversion. *Green Chemistry* **2018,** *20* (4), 921-934. https://doi.org/10.1039/C7GC03518G

32. Lau, C.-S.; Bunnell, K.; Carrier, D. J., Kinetic modeling of switchgrass-derived xylose oligomers degradation during pretreatment in dilute acid or in water. *ACS Sustainable Chemistry & Engineering* **2015,** *3* (9), 2030-2035. https://doi.org/10.1021/acssuschemeng.5b00298
33. Lau, C.-S.; Thoma, G. J.; Clausen, E. C.; Carrier, D. J., Kinetic Modeling of Xylose Oligomer Degradation during Pretreatment in Dilute Acid or in Water. *Industrial & Engineering Chemistry Research* **2014,** *53* (6), 2219-2228. https://doi.org/10.1021/ie403722d
34. Muller, F. O.; Manet, S.; Jean, B.; Chambat, G.; Boué, F. O.; Heux, L.; Cousin, F., SANS measurements of semiflexible xyloglucan polysaccharide chains in water reveal their self-avoiding statistics. *Biomacromolecules* **2011,** *12* (9), 3330-3336. https://doi.org/10.1021/bm200881x
35. Köhnke, T.; Östlund, Å.; Brelid, H., Adsorption of arabinoxylan on cellulosic surfaces: influence of degree of substitution and substitution pattern on adsorption characteristics. *Biomacromolecules* **2011,** *12* (7), 2633-2641. https://doi.org/10.1021/bm200437m
36. Sannigrahi, P.; Kim, D. H.; Jung, S.; Ragauskas, A., Pseudo-lignin and pretreatment chemistry. *Energy & Environmental Science* **2011,** *4* (4), 1306-1310. https://doi.org/10.1039/C0EE00378F
37. Kumar, R.; Hu, F.; Hubbell, C. A.; Ragauskas, A. J.; Wyman, C. E., Comparison of laboratory delignification methods, their selectivity, and impacts on physiochemical characteristics of cellulosic biomass. *Bioresource Technology* **2013,** *130*, 372-381. https://doi.org/10.1016/j.biortech.2012.12.028

Table of Content Figure (TOC Figure)
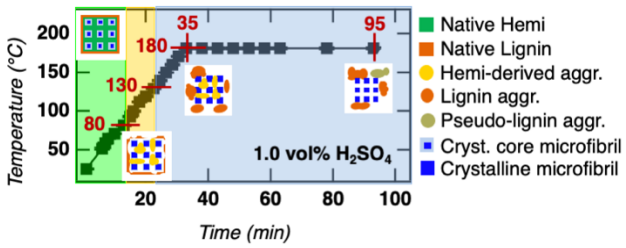
TOC Synopsis: Order of structural and morphological changes of the non-cellulosic plant polymers in switchgrass cell wall during dilute acid pretreatment.